

On Larger H_0 Values in the CMB Dipole Direction

Orlando Luongo,^{1,2,3,4,*} Marco Muccino,^{3,4,5,†} Eoin Ó Colgáin,^{6,7,‡} M. M. Sheikh-Jabbari,^{8,§} and Lu Yin^{6,7,¶}

¹*Dipartimento di Matematica, Università di Pisa, Largo B. Pontecorvo 5, Pisa, 56127, Italy.*

²*Divisione di Fisica, Università di Camerino, Via Madonna delle Carceri, 9, 62032, Italy.*

³*Al-Farabi Kazakh National University, Al-Farabi av. 71, 050040 Almaty, Kazakhstan.*

⁴*National Nanotechnology Laboratory of Open Type, Almaty 050040, Kazakhstan.*

⁵*Istituto Nazionale di Fisica Nucleare (INFN), Laboratori Nazionali di Frascati, 00044 Frascati, Italy.*

⁶*Center for Quantum Spacetime, Sogang University, Seoul 121-742, Korea.*

⁷*Department of Physics, Sogang University, Seoul 121-742, Korea.*

⁸*School of Physics, Institute for Research in Fundamental Sciences (IPM), P.O.Box 19395-5531, Tehran, Iran.*

On the assumption that quasars (QSO) and gamma-ray bursts (GRB) represent *standardisable candles*, we provide evidence that the Hubble constant H_0 adopts larger values in hemispheres aligned with the CMB dipole direction. This trends signals a departure from FLRW cosmology. In particular, QSOs show a definite trend, whereas the significance of the same statement in GRBs is sample dependent. Combining with similar trends in strong lensing, Type Ia supernovae (SN), the significance is the overall trend is in the 2.4σ - 4.5σ window, depending on the combination of data and openness to new cosmological probes. Our findings are consistent with reported discrepancies in the cosmic dipole and anisotropies in galaxy cluster scaling relations. The reported variations in H_0 across the sky suggest that Hubble tension is a symptom of a deeper cosmological malaise.

I. INTRODUCTION

Persistent cosmological tensions [1–7] suggest that it is timely to reflect on the success of the flat Λ CDM cosmology based on Planck values [8]. In particular, a $\sim 10\%$ discrepancy in the scale of the Hubble parameter in the post Planck era, *if true*, belies the moniker “precision cosmology”. Recently, the community has gone to considerable efforts to address these discrepancies (see [9]), but proposals are often physically contrived. Great progress has been made in cosmology through the *assumption* that the Universe is isotropic and homogeneous, namely the Cosmological Principle or Friedmann-Lemaître-Robertson-Walker (FLRW) paradigm. Nevertheless, cosmological tensions point to something being amiss. Here, we present evidence that FLRW is suspect [10] (see [11] for earlier comments).

The Cosmic Microwave Background (CMB) dipole is almost ubiquitously assumed to be of kinematical origin, i. e. due to relative motion. By subtracting the dipole, the CMB is defined as the rest frame for the Universe. CMB anomalies have been documented in [12] and some refer to anomalies with directional dependence, for example the (planar) alignment of the quadrupole and octopole and their normals with the CMB dipole [13, 14]. In addition, it has been argued that an anomalous parity asymmetry [15] may be traced to the CMB dipole [16, 17], so a common origin for CMB anomalies is plausible.

Separately, attempts to recover the CMB dipole from counts of late Universe sources such as radio galaxies [18–25] and QSOs [26], which are assumed to be in “CMB frame”, largely

agree that the CMB dipole direction is recovered, *but not the magnitude*. The implication is that observables in the late Universe are not in the same FLRW Universe. Independently, similar findings have emerged from studies of the apparent magnitudes of Type Ia supernovae (SN) [27] and QSOs [28]. In contrast, internal analysis of CMB data confirms the CMB dipole magnitude, but with large errors that allow an intrinsic (non-kinematic) component [29, 30].¹ It should be stressed that these results are based on partial sky coverage and this is a potential systematic.

Without doubt, the bread and butter of FLRW cosmology is the Hubble parameter $H(z)$. In particular, Hubble tension [1–5] casts a spotlight on $H_0 = H(z = 0)$. Here, we build on earlier observations for strongly lensed QSOs [10] and Type Ia SN [35] that H_0 values in the direction of the CMB dipole, loosely defined, are larger with significance 2.4σ . Similar variations of H_0 across the sky have been reported for scaling relations in galaxy clusters [36, 37].² Note, within FLRW the value of H_0 is insensitive to the number of observables in any given direction, but of course the number of observables impacts the errors. Finally, a variation in H_0 across the sky recasts the Hubble tension discussion [1–5] as a symptom of a deeper issue.

Our findings are that QSOs and GRBs, on the assumption that they represent *standardisable candles* [38–48], return higher H_0 values in hemispheres aligned with the CMB dipole direction. See also [49] for overlapping analysis. Admittedly, in contrast to Type Ia SN, QSOs and GRBs are non-standard, but *if* they are merely good enough to track H_0 , namely a universal constant in *all* FLRW cosmologies (see discussion in

*Electronic address: orlando.luongo@unicam.it

†Electronic address: muccino@lnf.infn.it

‡Electronic address: eoin@sogang.ac.kr

§Electronic address: shahin.s.jabbari@gmail.com

¶Electronic address: yinlu@sogang.ac.kr

¹ Interesting spatial dependence in the fine structure constant [31, 32] and alignments in QSO polarisations [33, 34] have been reported elsewhere. The latter define an axis closely aligned with the CMB dipole.

² Curiously, [36, 37] find that H_0 is lower along the CMB dipole direction, but restrict Ω_m to a Planck value in the analysis. This difference is worth investigating.

[50]), then we arrive at results that are at odds with FLRW. We emphasise that the physics of strong lensing time delay, Type Ia SN, QSOs and GRBs are sufficiently different with varying systematics. We quantify the significance of these observations by adopting different combinations of data, different redshift ranges and different orientations (that are expected to be irrelevant in a strict FLRW sense) arriving at significances in the range $2.4\sigma - 4.5\sigma$, which are large enough not to be dismissed. In particular, the lower bound is conservative and rests solely on strong lensing [51, 52] and Pantheon Type Ia SN [53]. Once QSOs [54] are taken into account, the significance is in the $3 - 4\sigma$ window, while GRBs [55] potentially push this beyond 4σ . It is hence plausible that at cosmic distances in the redshift range $O(0.1) \lesssim z \lesssim O(1)$ (and possibly beyond) the Universe is anisotropic and we have a preferred direction along the CMB dipole.³ As explained in [10], future observations of strongly lensed QSOs [51, 52] and potentially lensed SN [57] may settle the issue.

II. QSO DATA

QSOs as standardisable candles in cosmology would be a game changer, since they are plentiful even up to redshift $z \sim 7$. Despite a number of competitive proposals, e. g. [58–60] (see also [61, 62]), arguably the simplest and most powerful approach, due to Risaliti & Lusso [48], exploits an empirical relation between X-ray and UV luminosities in QSOs [63],

$$\log_{10} L_X = \beta + \gamma \log_{10} L_{UV}, \quad (1)$$

where β and $\gamma \approx 0.6$ are constants. Various studies have shown the robustness of the slope γ over both orders of magnitude in luminosity and extended redshift ranges [64–68]. The program [48, 54, 69, 70] is still in its infancy and reminiscent of the status of Type Ia SN in the 1990s [71]. The results so far have been intriguing, especially since they are at odds with Planck- Λ CDM [8].

In particular, QSOs (and GRBs) prefer larger values of matter density Ω_m , consistent with a Universe with little or no dark energy [72–75].⁴ This is due to a preference within QSOs for lower luminosity distances $D_L(z)$ relative to Planck- Λ CDM [8], especially at higher redshifts. Interestingly, Lyman- α BAO [77, 79] also prefers lower values of angular diameter distance $D_A(z) = (1+z)^{-2}D_L(z)$ and is therefore consistent with the Risaliti-Lusso QSOs⁵. Separately, it has been argued that best fit values of β, γ may be sensitive to the cosmological model, suggesting they should only be employed over restricted redshift ranges [80] or with QSO subsamples [81]. We address this concern in section IID.

A. Methods

The key idea of Risaliti & Lusso [48] is to assume that the relation (1) holds, before converting it into a relation in UV and X-ray fluxes, F_{UV} and F_X , respectively:

$$\log_{10} F_X = \beta + \gamma \log_{10} F_{UV} + (\gamma - 1) \log_{10}(4\pi D_L^2). \quad (2)$$

In a flat cosmology, $D_L(z)$ may be expressed as

$$D_L(z) = c(1+z) \int_0^z \frac{1}{H(z')} dz'. \quad (3)$$

Owing to the scatter in the QSO data, an additional intrinsic dispersion parameter δ is considered [48]. Thus, within the flat Λ CDM model, in addition to two cosmological parameters, (H_0, Ω_m) , there are three extra parameters: β, γ from (2) and δ . However, β is degenerate with $\log_{10} H_0$, so both cannot be independently determined without external data. Here we do not combine data sets, as the poorer quality QSO data risks returning unrepresentative values [72] and the goal is to extract information from QSOs directly. Due to this degeneracy we may fix H_0 to a canonical value, e.g. $H_0 = 70$ km/s/Mpc. In our analysis here we mainly focus on variation of quantity over putative hemispheres in the sky, which for observable X will be denoted by ΔX . From (2) one observes that $\Delta\beta \propto \Delta H_0/H_0$. Since $\gamma \approx 0.6 < 1$, the proportionality factor is positive, i.e. an *increase* in β maps over into an *increase* in H_0 .

The best-fit parameters $(\Omega_m, \beta, \gamma, \delta)$ follow from extremising the likelihood function [48],

$$\mathcal{L} = -\frac{1}{2} \sum_{i=1}^N \left[\frac{(\log_{10} F_{X,i}^{\text{obs}} - \log_{10} F_{X,i}^{\text{model}})^2}{s_i^2} + \ln(2\pi s_i^2) \right], \quad (4)$$

where $s_i^2 = \sigma_i^2 + \delta^2$ contains the measurement error on the observed flux $\log_{10} F_{X,i}^{\text{obs}}$ and δ . $\log_{10} F_{X,i}^{\text{model}}$ carries information about the cosmological model through (2).

On the data side, we make use of the latest compilation of QSO data [54], which contains 2421 QSOs in the redshift range $0.009 \leq z \leq 7.5413$. We show the redshift distribution of the full QSO sample and its distribution on the sky in FIG. 1 and FIG. 2. Evidently, the data becomes sparse as one approaches $z = 4$, while it is noticeable that the majority of the QSOs, 1655 in fact, are located in the range $90^\circ < \text{RA} < 270^\circ$ and in the northern hemisphere, $\text{DEC} > 0^\circ$. As explained in [54], while one can use the overall data set, the UV fluxes for some $z < 0.7$ QSOs have been determined by extrapolation from the optical, however there are some local QSOs, $z < 0.1$, whose UV spectra have been determined without extrapolation and one can have greater confidence in them. While one can include the local QSOs, it is conservative to remove all the QSOs below $z = 0.7$ [54] and this reduces the sample to 2023 QSOs. Observe that $z = 0.7$ is large enough that all the QSOs are expected to be in the same FLRW Universe as the CMB. Peculiar velocities are not relevant.

³ Note, it is already an established fact that at lower redshifts, in particular distances out to 200 Mpc, the local Universe is anisotropic, e. g. [56].

⁴ As explained in [76], the results of [54, 69, 70] have been negatively impacted by the cosmographic expansion, so claims of discrepancies in Ω_m cannot be substantiated without outside analysis.

⁵ The DES collaboration has also recently reported lower values of $D_A(z)$ at an effective redshift of $z_{\text{eff}} = 0.835$ through a blind analysis [78].

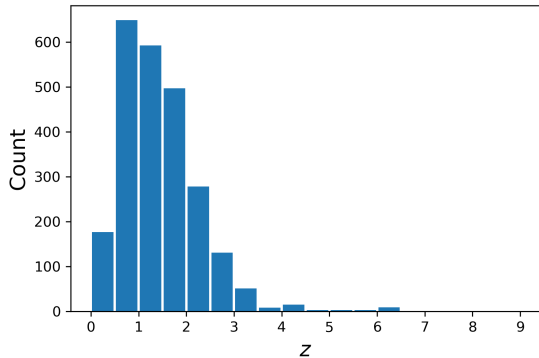


FIG. 1: The redshift distribution of the 2421 QSOs from the recent compilation [54] in intervals of $\Delta z = 0.5$.

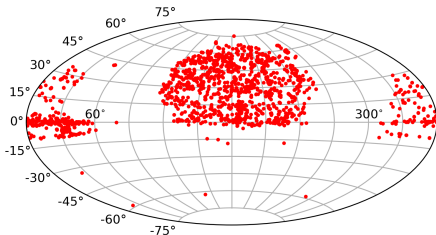


FIG. 2: Distribution of the QSOs [54] on the sky.

B. Analysis

We start by performing a consistency check in a bid to recover results quoted in [80]. To that end, we retain the local QSOs, $z < 0.1$, which we combine with QSOs in the redshift range $0.7 < z < 1.479$.⁶ Throughout we use the flat priors $0 \leq \Omega_m \leq 1$, $0 < \beta < 15$, $0 < \gamma < 1$ and $0 < \delta < 1$. As is clear from Table I, the results of extremisation and MCMC agree well, modulo the fact that Ω_m is displaced to smaller values. We have checked that the best-fit Ω_m value corresponds to the peak of the distribution, at least within the bounds, which means once restricted to the range $0 \leq \Omega_m \leq 1$, the distribution is lopsided, so the percentiles are shifted to smaller values. In effect, Ω_m wants to exceed the bound in order to reduce $D_L(z)$, but within flat Λ CDM, it cannot. Thus, displacements in MCMC values of Ω_m are an artefact of the bounds, otherwise extremisation and MCMC show good agreement. Finally, we can compare the results from [80], reproduced in Table I and confirm that there is agreement, despite a slight difference in data (see footnote 6).

⁶ In the data set downloaded from Vizier, we are unable to find the last two entries in Table 2 of [54], otherwise we are using the same local QSOs.

Ω_m	β	γ	δ
0.843	9.110	0.589	0.238
$0.697^{+0.204}_{-0.238}$	$8.980^{+0.505}_{-0.531}$	$0.594^{+0.017}_{-0.016}$	$0.239^{+0.006}_{-0.006}$
0.800	8.695	0.584	0.238
$0.670^{+0.300}_{-0.130}$	$8.570^{+0.530}_{-0.530}$	$0.588^{+0.018}_{-0.018}$	$0.239^{+0.006}_{-0.006}$

TABLE I: The best-fit values of the parameters for QSOs in the redshift range $0 < z < 0.1 \cup 0.7 < z < 1.479$. The first line corresponds to extremising the likelihood (4), whereas the second follows from an MCMC exploration, where we quote 1σ confidence intervals. The third and fourth lines record the analogous results from [80], modulo a slight difference in data (footnote 6).

The take away from the warmup exercise is that both extremisation and MCMC return consistent values of β . For us this is important, as we will explore variations of β across the sky by scanning over RA, DEC and using extremisation to identify differences in absolute β values between hemispheres. Extremisation with a focus on β is considerably quicker than MCMC, or fitting the logarithm dressed H_0 , and once the variations in β have been identified, we drill down on the more interesting orientations using MCMC in order to quantify the errors and extract the significance of any discrepancy. Concretely, we break the sky up into a 31×15 grid. Each point on this grid corresponds to two angles, which can be traded for a vector [35],

$$\vec{v} = [\cos(\text{DEC}) \cos(\text{RA}), \cos(\text{DEC}) \sin(\text{RA}), \sin(\text{DEC})]. \quad (5)$$

Observe that one gets the antipodal point on the sky by flipping the sign of DEC and shifting RA by 180° , so by opting for an odd number of points in our grid, we include antipodal points. This duplication allows for consistency checks. Next, one separates the sample based on the sign of the inner product of this vector with the corresponding vector for each data point in the QSO sample. This splits the data into two hemispheres. Once done, one extremises the likelihood (4) for each hemisphere and records the difference between the “northern” (N) and “southern” (S) hemisphere, $\Delta\beta = \beta^N - \beta^S$.

The result of this scan over the angles is shown in FIG. 3, where we have included the CMB dipole direction (RA, DEC) = $(168^\circ, -7^\circ)$ for guidance, and used the python library *scipy* (*scipy.interpolate.griddata*) to perform a cubic interpolation in $\Delta\beta$. We have checked that - as also visible in Fig. 3 or Fig. 4 - the antipodal point on the sky simply flips the sign of $\Delta\beta$. For this reason, the mean (and median) of our distribution in $\Delta\beta$ coincides with $\Delta\beta = 0$ and we have confirmed this is the case. In Table II we record the best-fit parameters for the CMB dipole direction and the direction of maximum $\Delta\beta$, where we have suppressed δ as it shows little variation. Note, we only consider the maximum $\Delta\beta$ from the sampled points and not the interpolation.

As is clear from Table II, once again extremisation and MCMC show good agreement. We have randomly sampled other points to confirm that this agreement is more widespread. From the 1σ confidence intervals in Table II one can estimate the discrepancy in $\Delta\beta$ between hemispheres to be

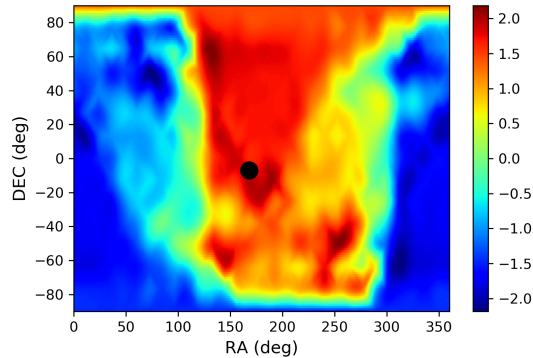


FIG. 3: Variations of the best-fit β parameters in respective hemispheres as (RA, DEC) values for the QSOs in the redshift range $0.7 < z \leq 7.5413$. The black dot denotes the CMB dipole. The lower (higher) β region corresponds to lower (higher) H_0 regions.

(RA, DEC)	Hemisphere	Ω_m	β	γ
CMB dipole	N	1	8.491	0.609
		$0.924^{+0.057}_{-0.107}$	$8.451^{+0.356}_{-0.371}$	$0.610^{+0.012}_{-0.011}$
	S	1	6.787	0.663
		$0.880^{+0.087}_{-0.155}$	$6.714^{+0.535}_{-0.538}$	$0.666^{+0.017}_{-0.017}$
(132°, 64.3°)	N	1	8.474	0.609
		$0.934^{+0.048}_{-0.096}$	$8.426^{0.354}_{-0.343}$	$0.611^{+0.011}_{-0.011}$
	S	1	6.291	0.679
		$0.845^{+0.114}_{-0.191}$	$6.171^{+0.633}_{-0.594}$	$0.683^{+0.019}_{-0.020}$

TABLE II: Best-fit values of the parameters from both extremisation and MCMC analysis of the likelihood (4) for QSOs in the redshift range $0.7 < z \leq 7.5413$.

2.7σ for the CMB dipole and 3σ for the maximum $\Delta\beta$. It is easy to check that both directions are in the same hemisphere using the vector inner product. These results may not be so surprising since we are working with the same tracer (QSOs) where a mismatch in the cosmic dipole has been reported with the CMB dipole at $\sim 5\sigma$ [26]. From our end, FIG. 3 is reminiscent of similar features in strong lensing time delay [10] and Type Ia SN [35].

We address caveats later in section IID where we comment on concerns that β evolves with redshift and varies across cosmological models [80]. However, here it is prudent to repeat our analysis in the more conservative redshift range $0.7 < z < 1.7$. The corresponding plot and results can be found in FIG. 4 and Table III. As expected, with the restricted redshift range, we reduce the QSO count to 1255, so this inflates the errors and reduces the significance. That being said, we still find a 2σ discrepancy for the CMB dipole and 2.8σ for the maximum $\Delta\beta$. Once again, these directions are in the same hemisphere. Interestingly, the maximum $\Delta\beta$ direction has flipped hemisphere, but this may be expected: FLRW H_0 is an extremely blunt probe of any anisotropy. Nevertheless,

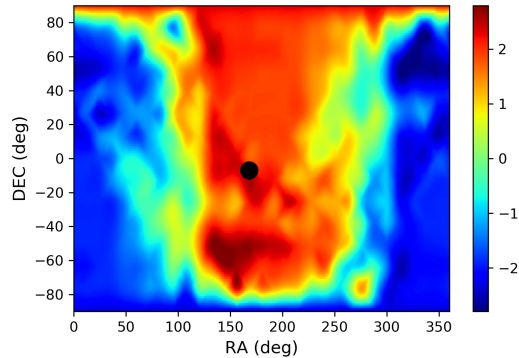


FIG. 4: Variations of the best-fit β parameters in respective hemispheres as (RA, DEC) values for the QSOs in the redshift range $0.7 < z < 1.7$. The black dot denotes the CMB dipole.

qualitatively FIG. 4 is the same as FIG. 3.

(RA, DEC)	Hemisphere	Ω_m	β	γ
CMB dipole	N	1	9.527	0.575
		$0.694^{+0.211}_{-0.261}$	$9.435^{+0.589}_{-0.573}$	$0.579^{+0.018}_{-0.019}$
	S	1	7.604	0.636
		$0.762^{+0.168}_{-0.273}$	$7.489^{+0.805}_{-0.788}$	$0.641^{+0.025}_{-0.026}$
(132°, -51.4°)	N	0.678	11.199	0.524
		$0.587^{+0.283}_{-0.294}$	$11.084^{+0.898}_{-0.917}$	$0.528^{+0.030}_{-0.028}$
	S	1	8.206	0.617
		$0.806^{+0.139}_{-0.214}$	$8.121^{+0.537}_{-0.563}$	$0.620^{+0.018}_{-0.017}$

TABLE III: Best-fit values of the parameters from both extremisation and MCMC analysis of the likelihood (4) for QSOs in the redshift range $0.7 < z < 1.7$.

C. Simulations

Taken at face value, FIG. 3 and FIG. 4 reveal striking emergent dipoles. As we have shown, one can find orientations in the sky where the variations in β , $\Delta\beta$, is significant. Nevertheless, this is an *a posteriori* inference. Here, we will attempt to quantify the significance through simulations based on the *a priori* assumption that the CMB dipole direction is relevant. Let us explain why this is the case. Recall that the CMB dipole has been subtracted on the assumption that it is purely kinematic in origin, i. e. due to relative motion. Existing results point to a persistent discrepancy in the cosmic dipole [18–28], which, if true, implies that CMB [8], radio galaxies [18–25], QSOs [26, 28] and Type Ia SN [27] do not inhabit the same FLRW frame. Our results are certainly consistent with this discrepancy. We are ultimately seeing that QSOs, which should be in the CMB rest frame, and thus ambivalent to the CMB dipole direction, are mysteriously tracking the CMB dipole direction.

It remains to see how unlikely this is in a representative flat Λ CDM Universe. To do so, we turn to simulations. Concretely, we first fix the redshift range, either $0.7 < z \leq 7.5413$ or $0.7 < z < 1.7$, and fit the flat Λ CDM model to the data to get an MCMC chain of representative values for $(\Omega_m, \beta, \gamma, \delta)$. As before, throughout we set $H_0 = 70$ km/s/Mpc. Next for each entry in the chain, we mock up new values of $\log_{10} F_{UV}$ by picking them randomly from normal distributions based on the corresponding error in $\log_{10} F_{UV}$. Here, the errors are typically small, so the new values are close to the original values of $\log_{10} F_{UV}$ and essentially all positive, $\log_{10} F_{UV} > 0$, as required. Next, we generate $\log_{10} F_X$ values consistent with equation (2) by employing $(\Omega_m, \beta, \gamma)$ from the MCMC chain to establish a mean value for $\log_{10} F_X$, before generating values in a normal distribution with standard deviation $s_i = \sqrt{\sigma_i^2 + \delta^2}$, where δ is also extracted from the MCMC chain. Doing this for entries in the MCMC chain, one builds up mock realisations of data that are consistent with both equation (2) and flat Λ CDM. We have checked that the mocking procedure typically returns values of $(\Omega_m, \beta, \gamma, \delta)$ within the 1σ confidence interval as defined by the MCMC chain.

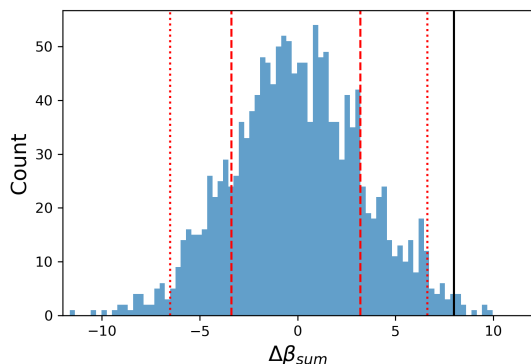


FIG. 5: The distribution of the weighted sum $\Delta\beta_{\text{sum}}$ for 1500 mock realisations of the real data from FIG. 3. The red dashed and dotted lines represent 1σ and 2σ , respectively, while the value for the real data, $\Delta\beta_{\text{sum}} = 7.98$, corresponds to the black line.

The question now is how often do figures such as FIG. 3 and FIG. 4 arise as statistical fluctuations? To answer this, we condense the heat maps into a number. Now, this number could be simply the discrepancy in β in a given direction, e. g. the CMB dipole direction, but it is better to focus on the hemisphere in the direction of the CMB dipole. The approach we adopt is to coarse grain our 31×11 grid to 11×5 , which once overlapping points at the boundary of the RA range are removed, leaves us with 50 equally spaced, distinct and *unassumingly* points on the sky. From these 50, by symmetry 25 will be in the same hemisphere as the CMB dipole. Now, one could simply sum the discrepancies in β at each point on the sky, i. e. $\sum_{i=1}^{25} \Delta\beta_i$, but it is better to introduce a weighting so that points on the sky that are closest to the CMB dipole direction contribute the most. The reason being that evidence suggests the matter dipole is not exactly aligned with the CMB dipole, e. g. [25, 26]. Therefore, our approach here is de-

signed to allow some ambiguity in the direction of any putative matter dipole provided it is close to the CMB dipole. Concretely, the proposal is to use the weighted sum,

$$\Delta\beta_{\text{sum}} = \sum_{i=1}^{25} w_i \Delta\beta_i, \quad (6)$$

where

$$w_i := \vec{v}_i \cdot \vec{v}_{\text{dipole}}, \quad (7)$$

and \vec{v}_{dipole} denotes the vector in the direction of the CMB dipole. Note that we have added the subscript “sum” to distinguish the weighted sum of $\Delta\beta_i$ and also that the inner product represents a natural way to weight the sum in the direction of the CMB dipole direction. This ensures dipoles that emerge as statistical fluctuations within the same hemisphere, *yet in directions other than the CMB dipole direction*, make a less significant contribution to the weighted sum.

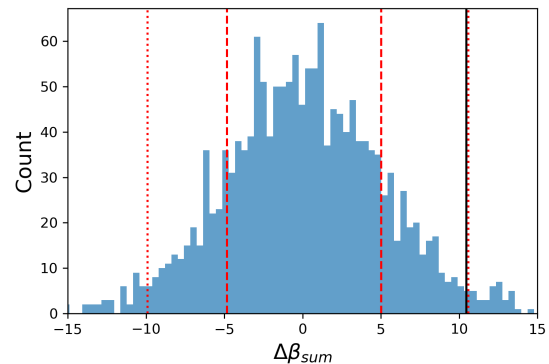


FIG. 6: The distribution of the weighted sum $\Delta\beta_{\text{sum}}$ for 1600 mock realisations of the real data from FIG. 4. The red dashed and dotted lines represent 1σ and 2σ , respectively, while the value for the real data, $\Delta\beta_{\text{sum}} = 10.45$, corresponds to the black line.

We now return to the original data and FIG. 3. For the full QSO sample in the range $0.7 < z \leq 7.5413$, we find $\Delta\beta_{\text{sum}} = 7.98$. In FIG. 5, we show the result of 1500 mock realisations of the data. From 1500 mock realisations, we find a larger value of the weighted sum in 11 cases, which represents a probability of $p = 0.007$ or 2.4σ for a single-sided Gaussian. This number can be compared with a 2.7σ discrepancy if we only focused on the CMB dipole direction (see Table II.) The significance is evident from the position of the black line relative to the 1σ and 2σ confidence intervals in FIG. 5. For the more conservative subsample in FIG. 4, the corresponding value of the weighted sum is $\Delta\beta_{\text{sum}} = 10.45$. From 1600 mock realisations of flat Λ CDM data, we find larger values of $\Delta\beta_{\text{sum}}$ in 40 realisations. This represents a probability of $p = 0.025$, or 2σ , to get a larger emergent dipole in the CMB dipole direction simply as a statistical fluctuation. This number can be compared with the 2σ discrepancy in the CMB dipole direction (see Table III). The realisations are plotted in FIG. 6, and once again, the statistical significance is visually evident.

D. Caveats

One caveat or feature of our QSO analysis is that it rests exclusively on flat Λ CDM. Since the QSO data returns large values of Ω_m , it is expected that changes in the dark energy model, which primarily affect low redshifts, do not affect β, γ and this can be confirmed from Table 3 of ref. [80]. In particular, observe that the β errors do not increase as the model changes, which implies that the significance of the deviation we see in flat Λ CDM will not change across dark energy models. However, introducing curvature Ω_k causes β to jump as is clear from a comparison of the ‘‘Flat Λ CDM’’ and ‘‘Non-flat Λ CDM’’ entries in Table 3 [80]. But this can be easily explained. As touched upon earlier, QSOs prefer smaller $D_L(z)$ values than Planck- Λ CDM. However, when one introduces curvature Ω_k , for $\Omega_k < 0$, a sine function appears in the definition of $D_L(z)$ - see e.g. eq.(9) of [80] - that is bounded above by unity. Thus, QSO data can exploit this bound and saturate to lower $D_L(z)$ values. This can lead to turning points in $H(z)$, as is clear from some of the results in [80].⁷ The jump in β can nonetheless be simply explained by the additional freedom beyond Ω_m , which the data gains to reduce $D_L(z)$, and increase $H(z)$, at higher z .

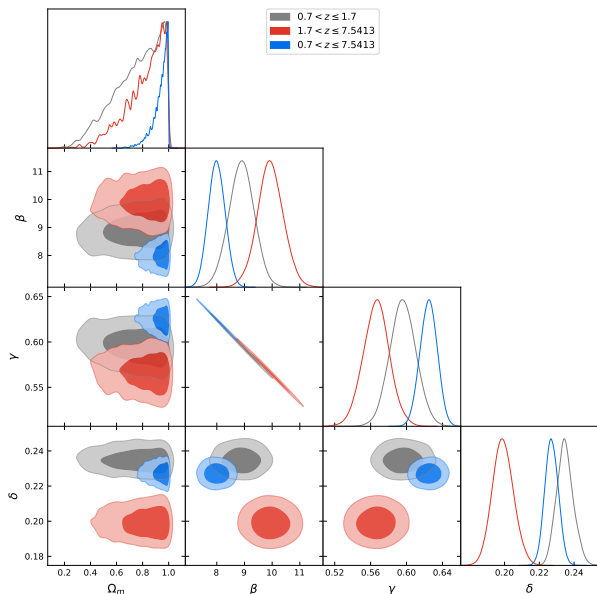


FIG. 7: Differences in the parameters Ω_m, β, γ and δ between low and high redshift samples. Here we made use of *getdist* [105].

A secondary caveat concerns the observation within flat Λ CDM that low and high redshift QSOs lead to inconsistent values when combined. Using the redshift $z = 1.7$ (in contrast to $z = 1.479$ [80]) as the border between low and high z , we confirm this in FIG. 7. Evidently, the red (high z) region

may be marginally discrepant with grey (low z), but our cut-off $z = 1.7$ is low enough that the grey and blue regions (all z) are more or less consistent. Interestingly, the intrinsic dispersion δ drops considerably at higher redshifts. This lower δ at higher redshift is also evident in Table 3 of [80]. This is expected as sparser high redshift data possesses less scatter, and with less data, results become less robust. Whether any evolution in (β, γ) is a physical feature or simply an artefact of high redshift data becoming sparse can be teased out with future QSO samples. That being said, there is no glaring inconsistency between grey and blue regions, so we are optimistic that both FIG. 3 and FIG. 4 are tracking H_0 appropriately.

In summary, we are seeing evidence for a higher value of H_0 within the flat Λ CDM model in the direction of the CMB dipole or aligned directions. Since we treat both hemispheres equally, there is no obvious bias. Indeed, FIG. 3 and FIG. 4 are reminiscent of similar features in strong lensing time delay [10] and Type Ia SN [35]. The naive interpretation is that there is a dipole anisotropy in the matter density of the Universe as traced by QSOs. This is consistent with the observation that there is a mismatch in the magnitude of the cosmic dipole between QSOs and CMB [26], but here (partial) sky coverage is not a concern.

III. GRBS

A. Uncalibrated GRBs

Our complementary analysis here is guided by the findings in [83], where assuming the Amati correlation [40], a compilation of 118 GRBs in the redshift range $0.3399 \leq z \leq 8.2$ with small enough intrinsic dispersion was identified. The relatively low scatter suggests that this sample may currently be the optimal one for cosmological studies. Given the improvement relative to previous samples, e. g. [55], it is interesting to see if GRBs, which are also high redshift probes, show the same feature as QSOs.

Recall that the Amati correlation relates the spectral peak energy in the GRB cosmological rest-frame $E_{p,i}$ and the isotropic energy E_{iso} :

$$\log_{10} E_{iso} = \alpha + \beta \log_{10} E_{p,i}, \quad (8)$$

where α and β are free parameters. Neither E_{iso} nor $E_{p,i}$ are observed quantities. The latter is related to the similar quantity in observer’s frame as $E_{p,i} = E_p^{obs}(1+z)$ and the former depends on the cosmology through the luminosity distance $D_L(z)$ and the measured bolometric fluence S_{bolo} [55],

$$E_{iso} = 4\pi D_L^2(z) S_{bolo} (1+z)^{-1}. \quad (9)$$

Once again we focus on flat Λ CDM and to address scatter in the GRB data, an intrinsic dispersion parameter δ is introduced. In line with previous analysis, we fix $H_0 = 70$ km/s/Mpc and adopt Ω_m, α, β and δ as the free parameters. The best-fit values are identified by extremising the following

⁷ See [82] for comments on turning points in $H(z)$ and implications for the Null Energy Condition.

likelihood function:

$$\mathcal{L} = -\frac{1}{2} \sum_{i=1}^N \left[\frac{(\log_{10} E_{\text{iso},i} - (\alpha + \beta \log_{10} E_{\text{p},i}))^2}{s_i^2} + \ln(2\pi s_i^2) \right], \quad (10)$$

where N is the number of GRBs. In addition, s_i depends on the S_{bolo} , $E_{\text{p},i}$, the corresponding errors $\sigma_{S_{\text{bolo}}}$, $\sigma_{E_{\text{p},i}}$ and the intrinsic dispersion,

$$s_i^2 = \left(\frac{\sigma_{S_{\text{bolo},i}}}{S_{\text{bolo},i} \ln(10)} \right)^2 + \beta^2 \left(\frac{\sigma_{E_{\text{p},i}}}{E_{\text{p},i} \ln(10)} \right)^2 + \delta^2. \quad (11)$$

We see from equation (8) that the degeneracy between H_0 and α means that an *increase* in H_0 corresponds to a *decrease* in α . Therefore, relative to QSOs, the degeneracy is opposite.

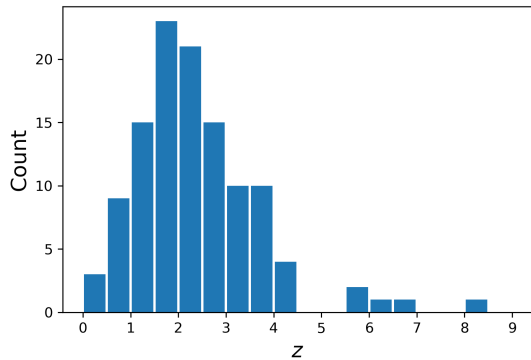


FIG. 8: Distribution of 118 GRBs with redshift z in intervals of $\Delta z = 0.5$.

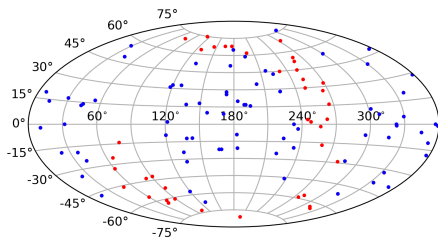


FIG. 9: Distribution of the 118 GRBs on the sky. Blue dots denote a subsample of 78 GRBs that are more closely aligned/misaligned with the CMB dipole with $|w_i| > 0.3$.

The methodology is the same as section II and the result of the scan over (RA, DEC) can be found in FIG. 10 and Table IV, where we record best-fit parameters for the CMB dipole direction and the direction of least $\Delta\alpha$. We suppress δ in Table IV as it consistently returns values in the vicinity of $\delta \approx 0.4$. Given that we have an order of magnitude fewer GRBs than QSOs, it is not surprising to see that any deviation in $\Delta\alpha$ is not

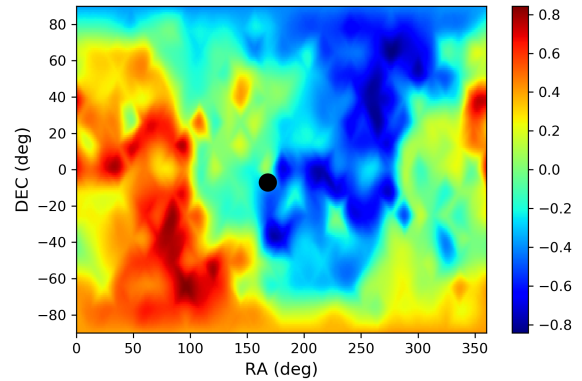


FIG. 10: Variations of the best-fit α parameter in respective hemispheres as (RA, DEC) values for the GRBs are scanned over. The black dot denotes the CMB dipole. Note that a higher (lower) value α corresponds to lower (higher) value H_0 .

so pronounced. From Table IV, we find that the discrepancy in α across hemispheres is 0.5σ for the CMB dipole and 1.6σ for the direction of minimum $\Delta\alpha$ (maximum $\Delta H_0/H_0$). Once again both vectors are in the same hemisphere and it is clear from the naked eye that FIG. 10 and 3 show similar regions on the sky where H_0 increases.

(RA, DEC)	Hemisphere	Ω_m	α	β
CMB dipole	N	1	49.83	1.17
		$0.67^{+0.23}_{-0.30}$	$49.91^{+0.40}_{-0.36}$	$1.20^{+0.13}_{-0.15}$
	S	0.38	50.22	1.08
		$0.52^{+0.32}_{-0.27}$	$50.17^{+0.30}_{-0.28}$	$1.08^{+0.10}_{-0.10}$
(264°, +64.3°)	N	1	49.61	1.23
		$0.64^{+0.25}_{-0.30}$	$49.72^{+0.36}_{-0.34}$	$1.24^{+0.12}_{-0.12}$
	S	0.72	50.46	0.96
		$0.60^{+0.27}_{-0.29}$	$50.49^{+0.34}_{-0.34}$	$0.98^{+0.13}_{-0.12}$

TABLE IV: Best-fit values of the parameters from both extremisation and MCMC analysis of the likelihood (10) for GRBs in the redshift range $0.3399 \leq z \leq 8.2$. Note, we quote the minimum value of $\Delta\alpha$ corresponding to the maximum value of ΔH_0 .

Given the size of the GRB sample, it is admittedly a little surprising that FIG. 10 shows good *qualitative* agreement with FIG. 3. However, this agreement may be deceiving and it is best once again to turn to simulations. Our methodology is as in section II, we use the weighted sum (6) except that here we track deviations in $\Delta\alpha$, $\Delta\alpha_{\text{sum}} = \sum_{i=1}^{25} w_i \Delta\alpha_i$. Once again, we perform an MCMC exploration of the original sample to identify representative values of $(\Omega_m, \alpha, \beta, \delta)$, and for each entry in the MCMC chain, we mock up new values of $E_{\text{p},i}$ by utilising the error $\sigma_{E_{\text{p},i}}$, before generating values of S_{bolo} , so that $E_{\text{iso},i}$ conform to the relation (8) with standard deviation s_i . For a number of these mock values, we have confirmed that the mock gives reasonable results in the sense that one is typically within the 1σ confidence intervals of the best-fit

parameters of $(\Omega_m, \alpha, \beta, \delta)$, as defined by the overall MCMC chain. Throughout, we have discarded any mocks with unphysical values of $E_{p,i}$, namely $E_{p,i} < 0$. This did not pose a problem with the earlier QSO mocks, but was a more prevalent problem here.

For the weighted sum evaluated on the real configuration in FIG. 10, we find $\Delta\alpha_{\text{sum}} = -0.92$. As expected, we see that the weighted sum returns a negative value consistent with a lower values of α and higher values of H_0 . Nevertheless, from 1432 mock realisations of the data, we find 1σ confidence intervals of $-2.09 < \Delta\alpha_{\text{sum}} < 2.44$ for the weighted sum. In particular, we find a lower value of $\Delta\alpha_{\text{sum}}$ in 433 cases, which means that the probability of a similar or lower value of $\Delta\alpha_{\text{sum}}$ arising simply by chance is $p = 0.30$. Therefore, the configuration in FIG. 10, while suggestive, is consistent with a statistical fluctuation within the flat Λ CDM model.

It should be noted that the intrinsic dispersion in the GRB sample, $\delta \sim 0.4$, is considerably larger than the QSO sample, $\delta \sim 0.24$. While one could attempt to reduce the scatter by hand by analysing the residuals from best-fit cosmologies and removing outliers, one can instead turn to orientation. Within the FLRW paradigm, it is assumed that orientation makes no difference. As a result, it is a valid exercise to consider the weight (7) and steadily remove GRBs with lower values of the absolute magnitude of w_i . This removes GRBs that are less closely aligned or misaligned with the CMB dipole. Thus, one can steadily remove GRBs with lower $|w_i|$, while documenting changes in $\Delta\alpha_{\text{sum}}$. In FIG. 11 we record a scan of the sky with 78 from the original 118 GRBs, where GRBs with $|w_i| < 0.3$ have been removed. The remaining GRBs are shown as blue dots in FIG. 9 and the corresponding value of the weighted sum is $\Delta\alpha_{\text{sum}} = -1.32$.

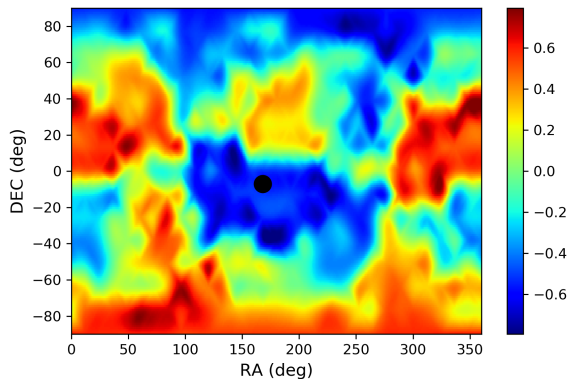


FIG. 11: Variations of the best-fit α parameter in respective hemispheres as (RA, DEC) values are scanned over. In contrast to FIG. 10, here we consider a subsample of 78 GRBs that are more closely aligned or misaligned with the CMB dipole. The black dot denotes the CMB dipole. Note that a higher (lower) value α corresponds to lower (higher) value H_0 .

Clearly, the dipole has become marginally more pronounced, but this is not enough to discern the real data in FIG. 11 from a statistical fluctuation within the flat Λ CDM model. In particular, we find that the 1σ confidence interval

for the weighted sum is $-2.74 < \Delta\alpha_{\text{sum}} < 3.6$ from 1511 mock realisations. Out of 1511 mocks, 456 lead to lower values of $\Delta\alpha_{\text{sum}}$ and this corresponds to a probability of $p = 0.30$, which makes the configuration in FIG. 11 indistinguishable from a statistical fluctuation. In summary, while the plots FIG. 10 and FIG. 11 are suggestive, they are consistent with statistical fluctuations and thereby largely inconclusive despite returning negative values of the weighted sum. While the analysis of removing GRBs with lower values of $|w_i|$ may seem redundant, since we do not see any noticeable effect, it serves as a prelude to similar analysis in the next subsection, where we do see a pronounced difference.

B. Calibrated GRBs

In this section we analyse a second compilation of 162 GRBs in the redshift range $0.03351 \leq z \leq 9.3$ that have been calibrated by Type Ia SN [55]. We remove all GRBs below $z = 0.3$ and this leaves us with 158 GRBs, which should be deep enough in redshift to share the same frame as the CMB. Since the data is in distance moduli, there are no nuisance parameters e. g. α, β, δ , and we can directly fit (H_0, Ω_m) to the distance moduli.

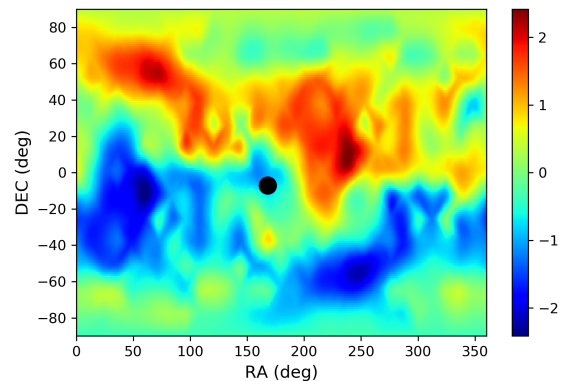


FIG. 12: Variations of (12) across the sky for 158 GRBs of [55] in the redshift range $0.3 < z \leq 9.3$.

Repeating the process outlined in the text with the full data set, while focusing on the (unweighted) hemisphere split quantity [35],

$$\sigma := (H_0^N - H_0^S) / \sqrt{(\delta H_0^N)^2 + (\delta H_0^S)^2}, \quad (12)$$

one arrives at FIG. 12. Note that in contrast to plots in the text, here the colour map is recording the significance of the discrepancy and not just the discrepancy. Obviously, this plot shows little or no correlation and is inconclusive. Moreover, in the CMB dipole direction H_0 is actually lower, thus contradicting our hypothesis. Nevertheless, we are encountering $\sim 2\sigma$ displacements at certain points on the sky.

In FIG. 13 we record the location of the GRBs on the sky. In contrast to the QSOs in FIG. 2 and smaller flux GRB sample in FIG. 9, one can see that the calibrated GRBs offer better

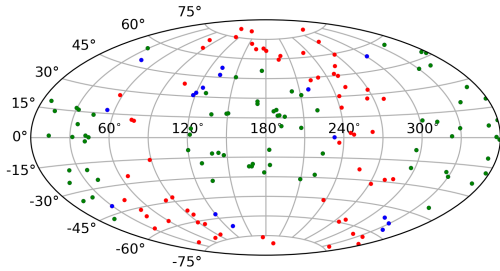


FIG. 13: Location of 158 GRBs in the redshift range $0.3 < z \leq 9.3$ [55] on the sky. The green dots denote a subsample of 78 GRBs with closest alignment/misalignment with the CMB dipole. Including the blue dots and red dots, one has 95 GRBs and 158 GRBs, respectively.

sky coverage. It is also worth stressing again that GRBs have a larger intrinsic dispersion, $\delta \sim 0.4$, relative to QSOs, $\delta \sim 0.23$. The other noticeable difference is the bunching in the QSO data away from the galactic plane. While the GRBs show no conclusive evidence for a dipole from FIG. 12, at least within an FLRW setup, as we have explained, one has the freedom to play with orientation, since it is not expected to make a difference. Thus, we can remove GRBs with smaller absolute values of the weight (7) and focus on GRBs that are more closely aligned or misaligned with the CMB dipole direction. Given the weight (7), one can define a weighted sum

$$\sigma_{\text{sum}} = \sum_i^{25} w_i \sigma_i, \quad (13)$$

where σ_i is defined in (12), and repeat the compression of heat maps into a number through the weighted sum. It appears that σ_{sum} is a better measure for anisotropy than $\Delta\alpha_{\text{sum}}$.

For the original 158 data points, we find that $\sigma_{\text{sum}} = -0.64$, thus reinforcing that, if anything, H_0 is lower in the CMB dipole direction, thus contradicting the working hypothesis. However, once the GRBs with $|w_i| < 0.4$ have been removed, this number changes dramatically to $\sigma_{\text{sum}} = 6.56$. The corresponding variation in H_0 with an interpolation based on the original 31×15 grid is shown in FIG. 14. The plot is in line with expectations once one notices that when we remove smaller values of $|w_i|$, we are left with fewer GRBs away from the CMB dipole axis and this explains the expansion in the light green regions where the discrepancy in H_0 is negligible. It should be stressed that although we have trimmed the data set to get this pronounced dipole, some of the features are still evident in the original plot, FIG. 12, including the dark red region at $(\text{RA}, \text{DEC}) \sim (240^\circ, 10^\circ)$ and the extension of the red region to the upper left corner.

We can now establish the significance of FIG. 14 by mocking up data consistent with flat Λ CDM using the same 95 data points. Concretely, we adopt the redshifts and errors on the distance moduli, but mock up the distance moduli from

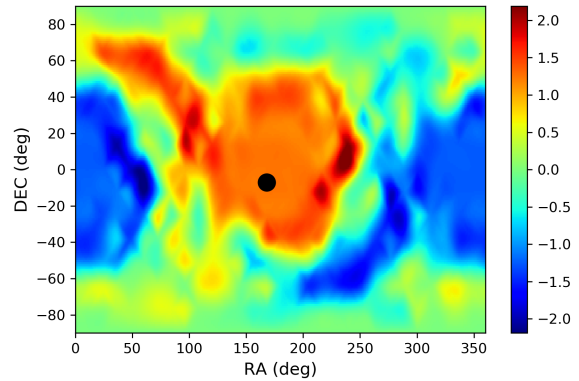


FIG. 14: Variations of (12) across the sky for a 95 GRB subsample of the GRBs of ref. [55]. We have removed GRBs less closely aligned or misaligned with the CMB dipole direction with $|w_i| < 0.4$

a normal distribution in (H_0, Ω_m) around the best-fit values, $H_0 = 73.01 \pm 11.81$ km/s/Mpc and $\Omega_m = 0.23 \pm 0.19$. From 2616 mock realisations, as illustrated in FIG. 15, we find 238 with larger values of σ_{sum} . Thus the probability of getting a more pronounced discrepancy in H_0 in the CMB dipole direction is $p = 0.091$. This represents 1.3σ for a single-sided Gaussian, which is consistent with the solid black line in FIG. 15.

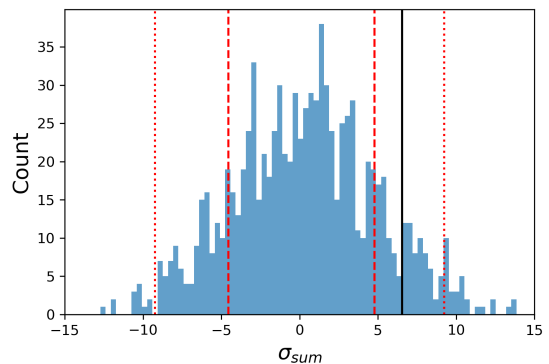


FIG. 15: The distribution of the weighted sum σ_{sum} for 2616 mock realisations of the real data from FIG. 14. The red dashed and dotted lines represent 1σ and 2σ , respectively, while the value for the real data, $\sigma_{\text{sum}} = 6.56$ corresponds to the black line.

We can consider a further cut by removing GRBs with $|w_i| < 0.5$, which leaves us with 78 GRBs. From FIG. 16 we can see that in contrast to FIG. 14, the red region has become a little deeper in colour. Using the reduced grid and weighted sum over 25 points in the same hemisphere as the CMB dipole direction, the sum increases from $\sigma_{\text{sum}} = 6.56$ to $\sigma_{\text{sum}} = 7.98$. Clearly, the emergent dipole has become more pronounced. Once again, we identify the best-fit parameters, $H_0 = 79.57 \pm 12.95$ km/s/Mpc and $\Omega_m = 0.23 \pm 0.16$ and construct 2575 mock realisations of the data. We find that 121 of these realisations lead to larger values of σ_{sum} . As a result, the

probability of a similar weighted sum arising by chance from within flat Λ CDM is $p = 0.047$, or 1.7σ for a single-sided Gaussian. The mocks are shown in FIG. 17.

In summary, we have seen how a relatively strong dipole can emerge from a calibrated GRB sample as the GRBs poorly aligned/misaligned with the CMB dipole direction are removed. It should be stressed that while there may be hidden correlations, and this point certainly deserves further study, *a priori* since we are working within an FLRW framework, the removal of GRBs in certain directions is not expected to greatly change the results. Nevertheless, as we have seen, once the poorly aligned/misaligned GRBs are removed, we see that the sample comprises higher (lower) values of H_0 in directions aligned (misaligned) with the CMB dipole. The expanding light green regions in FIG. 14 and FIG. 16 point to the same fact, namely in directions away from the CMB dipole, where we have removed GRBs, any differences in H_0 are minimal. Evidently, this is because one may be picking GRBs pretty evenly from samples of GRBs that prefer higher and lower H_0 values, respectively. Given that we have seen little change in the uncalibrated GRBs, but here the change is pronounced as we remove GRBs, it will be interesting to see if this effect is due to the calibration process with respect to Type Ia SN, since a similar emergent dipole has been observed there too [35]. We leave this question to future work.

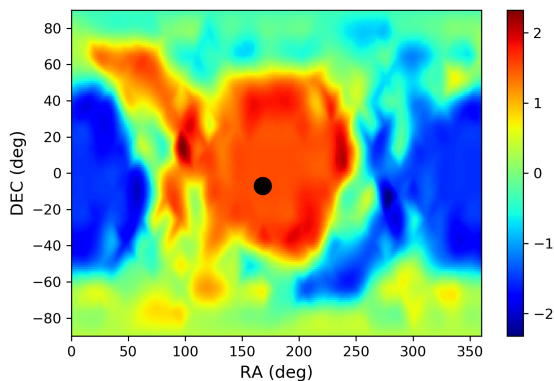


FIG. 16: Variations of (12) across the sky for a 78 GRB subsample of the GRBs of ref. [55]. We have removed GRBs less aligned or misaligned with the CMB dipole with $|w_l| < 0.5$.

IV. DISCUSSION

Building on earlier observations in strong lensing time delay [10] and Type Ia SN [35], which already place the significance at 2.4σ , we find independent evidence in QSOs and GRBs that H_0 is larger in the CMB dipole direction or aligned directions. Note that we have simply assumed the flat Λ CDM model, which *a priori* has no directional preference and knows nothing about any anisotropy. We focus on H_0 , since H_0 is a universal constant in any FLRW cosmology (for example, see [50]). For this reason, one expects all trends to be robust across cosmological models, although significance

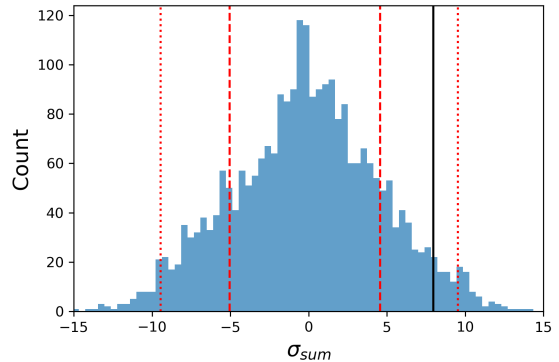


FIG. 17: The distribution of the weighted sum σ_{sum} for 2575 mock realisations of the real data from FIG. 16. The red dashed and dotted lines represent 1σ and 2σ , respectively, while the value for the real data, $\sigma_{\text{sum}} = 7.98$ corresponds to the black line.

may vary. The focus on H_0 also allows us to highlight H_0 , the local value of which is the subject of ongoing debate [1–5], but if our findings hold up, then there is no reason for H_0 in an FLRW context to be unique. In essence, “Hubble tension” may not be the problem it is usually stated to be.

It is certainly worth noting that despite working with proxy constants that are degenerate with H_0 , FIG. 3 and FIG. 10 negotiate signs to register good agreement across observables. Moreover, just as in the Hubble tension narrative, where one can replace H_0 with the absolute magnitude M_B of Type Ia SN to define “ M_B tension” [84, 85], one has the same freedom with β (for QSOs) and α (for GRBs). Given the small sample of GRBs, they simply play an accompanying role, but the significance of the deviation in the QSOs, as defined by our weighted sum (6), is $\geq 2\sigma$. Importantly, our lowest redshift QSO and GRB are sufficiently deep in redshift that within the usual FLRW framework all the data is expected to be in the CMB frame. Admittedly, since the GRB results are sample dependent, some further work is required to establish whether GRBs are contributing to a coherent narrative. Ultimately, this may have a simple explanation. For example, there is considerable scatter in GRB data sets and when the data is uncalibrated, one has to fit a large number of parameters.

Obviously, QSOs and GRBs are not widely used in cosmology, although this is changing in recent years [86–102]. Both have great potential as they probe redshift ranges not accessible by other probes. Nonetheless, they come with caveats, which we have openly discussed in section IID. Moreover, as we have shown here, when working with the latest QSO compilation [54] (see however [76]), one is implicitly working with a data set that is not only at odds with flat Λ CDM (large Ω_m), but also FLRW. As argued, this high redshift window in the late Universe is largely unexplored and even BAO has led to lower values of $D_A(z)$ [77, 78] that are consistent with the Risaliti-Lusso QSOs.

Given the diverse nature of the observables, e. g. $\log_{10} F_X$, $\log_{10} F_{UV}$, $E_{p,i}$ and S_{bolo} , there is nothing to suggest that we cannot simply multiply probabilities to ascertain the

probability that statistical fluctuations could explain our observation across strong lensing, Type Ia SN, QSOs and GRBs. Combining strong lensing, Type Ia SN and half the QSO sample, the significance is at 3.5σ (single-sided Gaussian). This increases marginally to 3.8σ with the full QSO sample. As we have seen, while analysis based on uncalibrated GRBs remains inconclusive, we are seeing a strong emergent dipole in calibrated GRBs. In particular, we identified 78 calibrated GRBs, where the probability of a fluke was $p = 0.047$. Folding this number into the probabilities, the statistical significance rises to 4.5σ , i. e. on par with any discrepancy in H_0 [1–5] and something not to be easily dismissed. This of course represents an optimistic assessment of the statistical significance pending a further study of GRB data. It should be stressed again that we have not employed any ansatz to guide the data, but simply worked within flat Λ CDM, so the observation that H_0 is higher across i) strong lensing time delay [10], ii) Type Ia SN [35], iii) QSOs and iv) GRBs, surely must have some interesting physical explanation. Obviously, a Universe with dipole anisotropy is the simplest interpretation and this claim can be tested by any competitive cosmological data set going forward. We have a prediction and as we gather more and better quality data the claim can either be true or false; our prediction has a good prospect to be verified but community engagement is required.

We close by briefly discussing the theoretical ramifications of our results. If further data confirms our findings, the simplest explanation may be that we have a preferred direction, aligned with the CMB dipole, in the Universe. That is, going to CMB rest-frame we see an anisotropic background. Homogeneous but anisotropic cosmologies are classified by Bianchi models. Since flat Λ CDM is apparently already a good approximation to the Universe, such Bianchi models should be anisotropic deviations from the flat Λ CDM. Moreover, our findings require the presence of a preferred “dipole” direction, which may be found in specific Bianchi models, such as the “tilted cosmology” of King and Ellis [103, 104]. Going beyond FLRW, one should revisit all the cosmological analyses and inferences, and write a new chapter in the cosmology book.

Acknowledgements

We thank Stephen Appleby, Narayan Khadka, Bharat Ratra and Jian-Min Wang for helpful discussions. We are grateful to Mohamed Rameez and Jenny Wagner for comments on a preliminary draft. We especially thank Chethan Krishnan and Roya Mohayaee for ongoing discussions on related topics. EOC is funded by the National Research Foundation of Korea (NRF-2020R1A2C1102899). MMSHJ would like to acknowledge SarAmadan grant No. ISEF/M/400122. LY was supported by the National Research Foundation of Korea funded through the CQeST of Sogang University (NRF2020R1A6A1A03047877). OL and MM acknowledge the Ministry of Education and Science of the Republic of Kazakhstan, Grant: IRN AP08052311.

Appendix A: Data

We record the GRB data compiled earlier in [83] in the below table. The QSO data [54] can be downloaded from <https://vizier.u-strasbg.fr/viz-bin/VizieR?-source=J/A+A/642/A150>.

TABLE V: The GRB data points

Name	Redshift z	E_p	S_{bolo}	RA	DEC
080916C	4.35	6953.87 ± 1188.77	10.40 ± 0.24	119.88	-57
090323	3.57	2060.09 ± 138.07	15.76 ± 0.39	190.69	17
090328	0.736	1221.71 ± 81.87	7.99 ± 0.20	90.87	-42
090424	0.544	236.91 ± 4.55	5.72 ± 0.09	189.54	17
090902B	1.822	2146.57 ± 21.71	39.05 ± 0.22	265.00	27
090926A	2.1062	868.63 ± 13.85	17.90 ± 0.13	353.25	-39
091003A	0.8969	857.81 ± 33.08	4.43 ± 0.08	251.50	37
091127	0.49	60.32 ± 1.93	2.25 ± 0.04	36.57	-19
091208B	1.063	202.63 ± 20.10	0.75 ± 0.04	29.41	17
100414A	1.368	1370.82 ± 27.68	11.88 ± 0.16	183.62	20
100728A	1.567	797.62 ± 18.05	11.74 ± 0.17	77.07	-14
110721A	3.512	8675.78 ± 852.66	6.14 ± 0.09	333.40	-39
120624B	2.2	1214.47 ± 26.24	20.49 ± 0.25	170.94	9
130427A	0.3399	294.25 ± 5.86	31.72 ± 0.20	173.14	28
130518A	2.49	1601.40 ± 32.19	11.40 ± 0.11	355.81	48
131108A	2.40	1163.20 ± 28.54	4.85 ± 0.05	156.47	10
131231A	0.6439	370.15 ± 4.97	17.42 ± 0.12	10.58	-2
141028A	2.33	1320.18 ± 50.90	4.89 ± 0.06	322.70	0
150314A	1.758	985.66 ± 13.20	9.20 ± 0.12	126.66	64
150403A	2.06	2428.51 ± 160.80	8.10 ± 0.17	311.50	-63
150514A	0.807	137.84 ± 14.93	0.71 ± 0.03	74.85	-61
160509A	1.17	19334.10 ± 652.25	49.91 ± 1.36	310.10	76
160625B	1.406	1546.86 ± 37.25	83.54 ± 1.16	308.27	7
170214A	2.53	2119.788 ± 119.06	22.40 ± 0.29	256.33	-2
170405A	3.51	1424.42 ± 35.24	9.24 ± 0.09	219.81	-25
971214	3.42	685.0 ± 133.0	0.87 ± 0.11	179.13	65
990123	1.6	1724.0 ± 466.0	35.80 ± 5.80	231.37	45
990510	1.619	423.0 ± 42.0	2.60 ± 0.40	204.53	-81
000131	4.5	987.0 ± 416.0	4.70 ± 0.80	93.39	-52
000926	2.07	310.0 ± 20.0	2.60 ± 0.60	256.06	52
010222	1.48	766.00 ± 30.0	14.6 ± 1.50	223.05	43
011211	2.14	186.0 ± 24.0	0.50 ± 0.06	168.82	-22
020124	3.2	448.0 ± 148.0	1.20 ± 0.10	143.28	-12
021004	2.3	266.0 ± 117.0	0.27 ± 0.04	6.73	19
030226	1.98	289.0 ± 66.0	1.30 ± 0.10	173.27	26
030323	3.37	270.0 ± 113.0	0.12 ± 0.04	166.53	-22
030328	1.52	328.00 ± 55.0	6.40 ± 0.60	182.69	-9
030429	2.65	128.0 ± 26.0	0.14 ± 0.02	183.28	-21
040912	1.563	44.00 ± 33.0	0.21 ± 0.06	359.00	-1
050318	1.44	115.00 ± 25.0	0.42 ± 0.03	49.68	-46
050401	2.9	467.0 ± 110.0	1.90 ± 0.40	247.88	2
050603	2.821	1333.0 ± 107.0	3.50 ± 0.20	39.98	-25
050820	2.612	1325.0 ± 277.0	6.40 ± 0.50	337.40	20
050904	6.29	3178 ± 1094.0	2.00 ± 0.20	13.67	14
050922C	2.198	415.0 ± 111.0	0.47 ± 0.16	317.39	-9
051109A	2.346	539.0 ± 200.0	0.51 ± 0.05	330.25	41
060115	3.53	285.0 ± 34.0	0.25 ± 0.04	54.05	17
060124	2.296	784.0 ± 285.0	3.40 ± 0.50	77.04	70
060206	4.048	394.0 ± 46.0	0.14 ± 0.03	202.95	35
060418	1.489	572.00 ± 143.0	2.30 ± 0.50	236.42	-4
060526	3.21	105.0 ± 21.0	0.12 ± 0.06	232.85	0
060707	3.425	279.0 ± 28.0	0.23 ± 0.04	357.08	-18

Name	redshift z	E_p	S_{bolo}	RA	DEC
060908	2.43	514.0 ± 102.0	0.73 ± 0.07	31.83	0
060927	5.6	475.0 ± 47.0	0.27 ± 0.04	329.55	5
070125	1.547	934.00 ± 148.0	13.30 ± 1.30	117.85	31
071003	1.604	2077 ± 286	5.32 ± 0.590	301.85	11
071020	2.145	1013.0 ± 160.0	0.87 ± 0.40	119.66	33
080319C	1.95	906.0 ± 272.0	1.50 ± 0.30	258.98	55
080413	2.433	584.0 ± 180.0	0.56 ± 0.14	287.29	-28
080514B	1.8	627.0 ± 65.0	2.027 ± 0.48	322.82	-1
080603B	2.69	376.0 ± 100.0	0.64 ± 0.058	176.53	68
080605	1.6398	650.0 ± 55.0	3.40 ± 0.28	262.13	4
080607	3.036	1691.0 ± 226.0	8.96 ± 0.48	194.97	16
080721	2.591	1741.0 ± 227.0	7.86 ± 1.37	224.47	-12
080810	3.35	1470.0 ± 180.0	1.82 ± 0.20	356.78	0
080913	6.695	710.0 ± 350.0	0.12 ± 0.035	65.73	-25
081008	1.9685	261.0 ± 52.0	0.96 ± 0.09	279.99	-57
081028	3.038	234.0 ± 93.0	0.81 ± 0.095	121.89	2
081118	2.58	147.0 ± 14.0	0.27 ± 0.057	82.59	-43
081121	2.512	47.23 ± 1.08	1.71 ± 0.33	89.26	-61
081222	2.77	505.0 ± 34.0	1.67 ± 0.17	22.75	-34
090102	1.547	1149.00 ± 166.0	3.48 ± 0.63	128.26	33
090418	1.608	1567 ± 384	2.35 ± 0.59	269.33	33
090423	8.2	491.0 ± 200.0	0.12 ± 0.032	148.90	18
090516	4.109	971.0 ± 390.0	1.96 ± 0.38	138.27	-12
090715B	3.0	536.0 ± 172.0	1.09 ± 0.17	251.35	45
090812	2.452	2000.0 ± 700.0	3.08 ± 0.53	353.20	-11
091020	1.71	280.0 ± 190.0	0.11 ± 0.034	175.72	51
091029	2.752	230.0 ± 66.0	0.47 ± 0.044	60.18	-56
100413	3.9	1783.60 ± 374.85	2.36 ± 0.77	266.00	16
100621	0.54	146.49 ± 23.9	5.75 ± 0.64	315.25	-51
100704	3.6	809.60 ± 135.70	0.70 ± 0.07	133.50	-24
100814	1.44	312.32 ± 48.8	1.39 ± 0.23	22.25	-18
100906	1.73	387.23 ± 244.07	3.56 ± 0.55	28.50	56
110205	2.22	740.60 ± 322.0	3.32 ± 0.68	164.50	68
110213	1.46	223.86 ± 70.11	1.55 ± 0.23	43.00	49
110422	1.77	421.04 ± 13.85	9.32 ± 0.02	111.75	75

110503	1.61	572.25 ± 50.95	2.76 ± 0.21	132.75	52
110715	0.82	218.40 ± 20.93	2.73 ± 0.24	237.50	-46
110731	2.83	1164.32 ± 49.79	2.51 ± 0.01	280.50	-29
110818	3.36	1117.47 ± 241.11	1.05 ± 0.08	317.25	-64
111008	5.0	894.00 ± 240.0	1.06 ± 0.11	60.25	-33
111107	2.89	420.44 ± 124.58	0.18 ± 0.03	129.25	-67
111209	0.68	519.87 ± 88.88	69.47 ± 8.72	14.25	-47
120119	1.73	417.38 ± 54.56	4.62 ± 0.59	120.00	-9
120326	1.8	129.97 ± 10.27	0.44 ± 0.02	273.75	69
120724	1.48	68.45 ± 18.60	0.15 ± 0.02	245.00	4
120802	3.8	274.33 ± 93.04	0.43 ± 0.07	44.75	14
120811C	2.67	157.49 ± 20.92	0.74 ± 0.07	199.71	62
120909	3.93	1651.55 ± 123.25	2.69 ± 0.23	275.50	-59
120922	3.1	156.62 ± 0.04	1.59 ± 0.18	234.75	-20
121128	2.2	243.20 ± 12.8	0.87 ± 0.07	300.50	54
130215	0.6	247.54 ± 100.61	4.84 ± 0.12	43.25	13
130408	3.76	1003.94 ± 137.98	0.99 ± 0.17	134.25	-32
130420A	1.3	128.63 ± 6.89	1.73 ± 0.06	196.10	59
130505	2.27	2063.37 ± 101.37	4.56 ± 0.09	137.00	17
130514	3.6	496.80 ± 151.8	1.88 ± 0.25	296.25	-8
130606	5.91	2031.54 ± 483.7	0.49 ± 0.09	249.25	30
130610	2.09	911.83 ± 132.65	0.82 ± 0.05	224.25	28
130612	2.01	186.07 ± 31.56	0.08 ± 0.01	259.75	-17
130701A	1.16	191.80 ± 8.62	0.46 ± 0.04	224.42	28
130831A	0.48	81.35 ± 5.92	1.29 ± 0.07	358.65	29
130907A	1.24	881.77 ± 24.62	75.21 ± 4.76	215.88	46

Name	redshift z	E_p	S_{bolo}	RA	DEC
131030A	1.29	405.86 ± 22.93	1.05 ± 0.10	345.08	-5
131105A	1.69	547.68 ± 83.53	4.75 ± 0.16	71.01	-63
131117A	4.04	221.85 ± 37.31	0.05 ± 0.01	332.34	-32
140206A	2.73	447.60 ± 22.38	1.69 ± 0.03	145.35	67
140213A	1.21	176.61 ± 4.42	2.53 ± 0.04	105.22	-73

- [1] A. G. Riess, S. Casertano, W. Yuan, J. B. Bowers, L. Macri, J. C. Zinn and D. Scolnic, *Astrophys. J. Lett.* **908** (2021) no.1, L6 [arXiv:2012.08534 [astro-ph.CO]].
- [2] W. L. Freedman, [arXiv:2106.15656 [astro-ph.CO]].
- [3] D. W. Pesce, J. A. Braatz, M. J. Reid, A. G. Riess, D. Scolnic, J. J. Condon, F. Gao, C. Henkel, C. M. V. Impellizzeri and C. Y. Kuo, *et al.* *Astrophys. J. Lett.* **891** (2020) no.1, L1 [arXiv:2001.09213 [astro-ph.CO]].
- [4] J. P. Blakeslee, J. B. Jensen, C. P. Ma, P. A. Milne and J. E. Greene, *Astrophys. J.* **911** (2021) no.1, 65 [arXiv:2101.02221 [astro-ph.CO]].
- [5] E. Kourkchi, R. B. Tully, G. S. Anand, H. M. Courtois, A. Dupuy, J. D. Neill, L. Rizzi and M. Seibert, *Astrophys. J.* **896** (2020) no.1, 3 [arXiv:2004.14499 [astro-ph.GA]].
- [6] T. M. C. Abbott *et al.* [DES], [arXiv:2105.13549 [astro-ph.CO]].
- [7] M. Asgari *et al.* [KiDS], *Astron. Astrophys.* **645** (2021), A104 [arXiv:2007.15633 [astro-ph.CO]].
- [8] N. Aghanim *et al.* [Planck], *Astron. Astrophys.* **641** (2020), A6 [arXiv:1807.06209 [astro-ph.CO]].
- [9] E. Di Valentino, O. Mena, S. Pan, L. Visinelli, W. Yang, A. Melchiorri, D. F. Mota, A. G. Riess and J. Silk, [arXiv:2103.01183 [astro-ph.CO]].
- [10] C. Krishnan, R. Mohayaee, E. Ó. Colgáin, M. M. Sheikh-Jabbari and L. Yin, *Class. Quant. Grav.* **38** (2021) no.18, 184001 [arXiv:2105.09790 [astro-ph.CO]].
- [11] P. Fleury, H. Dupuy and J. P. Uzan, *Phys. Rev. Lett.* **111** (2013), 091302 [arXiv:1304.7791 [astro-ph.CO]].
- [12] D. J. Schwarz, C. J. Copi, D. Huterer and G. D. Starkman, *Class. Quant. Grav.* **33** (2016) no.18, 184001 [arXiv:1510.07929 [astro-ph.CO]].
- [13] A. de Oliveira-Costa, M. Tegmark, M. Zaldarriaga and A. Hamilton, *Phys. Rev. D* **69** (2004), 063516 [arXiv:astro-ph/0307282 [astro-ph]].
- [14] D. J. Schwarz, G. D. Starkman, D. Huterer and C. J. Copi, *Phys. Rev. Lett.* **93** (2004), 221301 [arXiv:astro-ph/0403353 [astro-ph]].
- [15] K. Land and J. Magueijo, *Phys. Rev. D* **72** (2005), 101302 [arXiv:astro-ph/0507289 [astro-ph]].
- [16] J. Kim and P. Naselsky, *Astrophys. J. Lett.* **714** (2010), L265-L267 [arXiv:1001.4613 [astro-ph.CO]].
- [17] P. Naselsky, W. Zhao, J. Kim and S. Chen, *Astrophys. J.* **749** (2012), 31 [arXiv:1108.4376 [astro-ph.CO]].
- [18] C. Blake and J. Wall, *Nature* **416** (2002), 150-152

- [arXiv:astro-ph/0203385 [astro-ph]].
- [19] A. K. Singal, *Astrophys. J. Lett.* **742** (2011), L23 [arXiv:1110.6260 [astro-ph.CO]].
- [20] C. Gibelyou and D. Huterer, *Mon. Not. Roy. Astron. Soc.* **427** (2012), 1994-2021 [arXiv:1205.6476 [astro-ph.CO]].
- [21] M. Rubart and D. J. Schwarz, *Astron. Astrophys.* **555** (2013), A117 [arXiv:1301.5559 [astro-ph.CO]].
- [22] P. Tiwari and A. Nusser, *JCAP* **03** (2016), 062 [arXiv:1509.02532 [astro-ph.CO]].
- [23] J. Colin, R. Mohayaee, M. Rameez and S. Sarkar, *Mon. Not. Roy. Astron. Soc.* **471** (2017) no.1, 1045-1055 [arXiv:1703.09376 [astro-ph.CO]].
- [24] C. A. P. Bengaly, R. Maartens and M. G. Santos, *JCAP* **04** (2018), 031 [arXiv:1710.08804 [astro-ph.CO]].
- [25] T. M. Siewert, M. Schmidt-Rubart and D. J. Schwarz, [arXiv:2010.08366 [astro-ph.CO]].
- [26] N. J. Secrest, S. von Hausegger, M. Rameez, R. Mohayaee, S. Sarkar and J. Colin, *Astrophys. J. Lett.* **908** (2021) no.2, L51 [arXiv:2009.14826 [astro-ph.CO]].
- [27] A. K. Singal, [arXiv:2106.11968 [astro-ph.CO]].
- [28] A. K. Singal, [arXiv:2107.09390 [astro-ph.CO]].
- [29] P. d. Ferreira and M. Quartin, *Phys. Rev. Lett.* **127** (2021) no.10, 101301 [arXiv:2011.08385 [astro-ph.CO]].
- [30] S. Saha, S. Shaikh, S. Mukherjee, T. Souradeep and B. D. Wandelt, [arXiv:2106.07666 [astro-ph.CO]].
- [31] J. K. Webb, J. A. King, M. T. Murphy, V. V. Flambaum, R. F. Carswell and M. B. Bainbridge, *Phys. Rev. Lett.* **107** (2011), 191101 [arXiv:1008.3907 [astro-ph.CO]].
- [32] J. A. King, J. K. Webb, M. T. Murphy, V. V. Flambaum, R. F. Carswell, M. B. Bainbridge, M. R. Wilczynska and F. E. Koch, *Mon. Not. Roy. Astron. Soc.* **422** (2012), 3370-3413 [arXiv:1202.4758 [astro-ph.CO]].
- [33] D. Hutsemekers and H. Lamy, *Astron. Astrophys.* **367** (2001), 381-387 [arXiv:astro-ph/0012182 [astro-ph]].
- [34] D. Hutsemekers, R. Cabanac, H. Lamy and D. Sluse, *Astron. Astrophys.* **441** (2005), 915-930 [arXiv:astro-ph/0507274 [astro-ph]].
- [35] C. Krishnan, R. Mohayaee, E. Ó Colgáin, M. M. Sheikh-Jabbari and L. Yin, [arXiv:2106.02532 [astro-ph.CO]].
- [36] K. Migkas, G. Schellenberger, T. H. Reiprich, F. Pacaud, M. E. Ramos-Ceja and L. Lovisari, *Astron. Astrophys.* **636** (2020), A15 [arXiv:2004.03305 [astro-ph.CO]].
- [37] K. Migkas, F. Pacaud, G. Schellenberger, J. Erler, N. T. Nguyen-Dang, T. H. Reiprich, M. E. Ramos-Ceja and L. Lovisari, *Astron. Astrophys.* **649** (2021), A151 [arXiv:2103.13904 [astro-ph.CO]].
- [38] B. E. Schaefer, *Astrophys. J.* **660** (2007), 16.
- [39] F. Y. Wang, Z. G. Dai, and Z.-H. Zhu, *Astrophys. J.* **667** (2007), 1-10.
- [40] L. Amati, C. Guidorzi, F. Frontera, M. Della Valle, F. Finelli, R. Landi and E. Montanari, *Mon. Not. Roy. Astron. Soc.* **391** (2008), 577-584 [arXiv:0805.0377 [astro-ph]].
- [41] S. Capozziello, and L. Izzo, *Astronom. Astrophys.* **490** (2008), 31-36.
- [42] M. G. Dainotti, V. F. Cardone, and S. Capozziello, *Mon. Not. Roy. Astron. Soc.* **391** (2008), L79-L83.
- [43] L. Izzo, S. Capozziello, G. Covone, and M. Capaccioli, *Astronom. Astrophys.* **508** (2009), 63-67.
- [44] L. Amati and M. Della Valle, *International Journal of Modern Physics D* **22** (2013), 1330028.
- [45] J.-J. Wei, X.-F. Wu, F. Melia, D.-M. Wei, and L.-L. Feng, *Mon. Not. Roy. Astron. Soc.* **439** (2014), 3329-3341.
- [46] L. Izzo, M. Muccino, E. Zaninoni, L. Amati, and M. Della Valle, *Astronom. Astrophys.* **582** (2015), A115.
- [47] C.-H. Tang, Y.-F. Huang, J.-J. Geng, and Z.-B. Zhang, *Astrophys. J. Suppl.* **245** (2019), 1.
- [48] G. Risaliti and E. Lusso, *Astrophys. J.* **815** (2015), 33 [arXiv:1505.07118 [astro-ph.CO]].
- [49] D. Zhao and J. Q. Xia, *Eur. Phys. J. C* **81** (2021) no.8, 694
- [50] C. Krishnan, E. Ó Colgáin, M. M. Sheikh-Jabbari and T. Yang, *Phys. Rev. D* **103** (2021) no.10, 103509 [arXiv:2011.02858 [astro-ph.CO]].
- [51] K. C. Wong, S. H. Suyu, G. C. F. Chen, C. E. Rusu, M. Millon, D. Sluse, V. Bonvin, C. D. Fassnacht, S. Taubenberger and M. W. Auger, *et al.* *Mon. Not. Roy. Astron. Soc.* **498** (2020) no.1, 1420-1439 [arXiv:1907.04869 [astro-ph.CO]].
- [52] M. Millon, A. Galan, F. Courbin, T. Treu, S. H. Suyu, X. Ding, S. Birrer, G. C. F. Chen, A. J. Shajib and D. Sluse, *et al.* *Astron. Astrophys.* **639** (2020), A101 [arXiv:1912.08027 [astro-ph.CO]].
- [53] D. M. Scolnic, D. O. Jones, A. Rest, Y. C. Pan, R. Chornock, R. J. Foley, M. E. Huber, R. Kessler, G. Narayan and A. G. Riess, *et al.* *Astrophys. J.* **859** (2018) no.2, 101 [arXiv:1710.00845 [astro-ph.CO]].
- [54] E. Lusso, G. Risaliti, E. Nardini, G. Bargiacchi, M. Benetti, S. Bisogni, S. Capozziello, F. Civano, L. Eggleston and M. Elvis, *et al.* *Astron. Astrophys.* **642** (2020), A150 [arXiv:2008.08586 [astro-ph.GA]].
- [55] M. Demianski, E. Piedipalumbo, D. Sawant and L. Amati, *Astron. Astrophys.* **598** (2017), A112 [arXiv:1610.00854 [astro-ph.CO]].
- [56] Y. Hoffman, D. Pomarede, R. Brent Tully and H. Courtois, doi:10.1038/s41550-016-0036 [arXiv:1702.02483 [astro-ph.CO]].
- [57] S. H. Suyu, S. Huber, R. Cañameras, M. Kromer, S. Schuldt, S. Taubenberger, A. Yıldırım, V. Bonvin, J. H. H. Chan and F. Courbin, *et al.* *Astron. Astrophys.* **644** (2020), A162 [arXiv:2002.08378 [astro-ph.CO]].
- [58] D. Watson, K. D. Denney, M. Vestergaard and T. M. Davis, *Astrophys. J. Lett.* **740** (2011), L49 [arXiv:1109.4632 [astro-ph.CO]].
- [59] J. M. Wang, P. Du, D. Valls-Gabaud, C. Hu and H. Netzer, *Phys. Rev. Lett.* **110** (2013) no.8, 081301 [arXiv:1301.4225 [astro-ph.CO]].
- [60] F. La Franca, S. Bianchi, G. Ponti, E. Branchini and G. Matt, *Astrophys. J. Lett.* **787** (2014), L12 [arXiv:1404.2607 [astro-ph.CO]].
- [61] D. C. Dai, G. D. Starkman, B. Stojkovic, D. Stojkovic and A. Weltman, *Phys. Rev. Lett.* **108** (2012), 231302 [arXiv:1204.5191 [astro-ph.CO]].
- [62] R. Solomon and D. Stojkovic, [arXiv:2110.03671 [astro-ph.CO]].
- [63] H. Tananbaum, Y. Avni, G. Branduardi *et al.* *Astrophys. J.* **234** (1979) L9
- [64] C. Vignali, W. N. Brandt and D. P. Schneider, *Astron. J.* **125** (2003), 433 [arXiv:astro-ph/0211125 [astro-ph]].
- [65] D. W. Just, W. N. Brandt, O. Shemmer, A. T. Steffen, D. P. Schneider, G. Chartas and G. P. Garmire, *Astrophys. J.* **665** (2007), 1004-1022 [arXiv:0705.3059 [astro-ph]].
- [66] E. Lusso, A. Comastri, C. Vignali, G. Zamorani, M. Brusa, R. Gilli, K. Iwasawa, M. Salvato, F. Civano and M. Elvis, *et al.* *Astron. Astrophys.* **512** (2010), A34 [arXiv:0912.4166 [astro-ph.CO]].
- [67] F. Salvestrini, G. Risaliti, S. Bisogni, E. Lusso and C. Vignali, *Astron. Astrophys.* **631** (2019), A120 [arXiv:1909.12309 [astro-ph.GA]].
- [68] S. Bisogni, E. Lusso, F. Civano, E. Nardini, G. Risaliti, M. Elvis and G. Fabbiano, [arXiv:2109.03252 [astro-ph.GA]].

- [69] G. Risaliti and E. Lusso, *Nature Astron.* **3** (2019) no.3, 272-277 [[arXiv:1811.02590](#) [astro-ph.CO]].
- [70] E. Lusso, E. Piedipalumbo, G. Risaliti, M. Paolillo, S. Bisogni, E. Nardini and L. Amati, *Astron. Astrophys.* **628** (2019), L4 [[arXiv:1907.07692](#) [astro-ph.CO]].
- [71] M. M. Phillips, *Astrophys. J. Lett.* **413** (1993), L105-L108
- [72] T. Yang, A. Banerjee and E. Ó Colgáin, *Phys. Rev. D* **102** (2020) no.12, 123532 [[arXiv:1911.01681](#) [astro-ph.CO]].
- [73] H. Velten and S. Gomes, *Phys. Rev. D* **101** (2020) no.4, 043502 [[arXiv:1911.11848](#) [astro-ph.CO]].
- [74] N. Khadka and B. Ratra, *Mon. Not. Roy. Astron. Soc.* **492** (2020) no.3, 4456-4468 [[arXiv:1909.01400](#) [astro-ph.CO]].
- [75] N. Khadka and B. Ratra, *Mon. Not. Roy. Astron. Soc.* **497** (2020) no.1, 263-278 [[arXiv:2004.09979](#) [astro-ph.CO]].
- [76] A. Banerjee, E. Ó Colgáin, M. Sasaki, M. M. Sheikh-Jabbari and T. Yang, *Phys. Lett. B* **818** (2021), 136366 [[arXiv:2009.04109](#) [astro-ph.CO]].
- [77] T. Delubac *et al.* [BOSS], *Astron. Astrophys.* **574** (2015), A59 [[arXiv:1404.1801](#) [astro-ph.CO]].
- [78] T. M. C. Abbott *et al.* [DES], [[arXiv:2107.04646](#) [astro-ph.CO]].
- [79] H. du Mas des Bourboux, J. Rich, A. Font-Ribera, V. de Sainte Agathe, J. Farr, T. Etourneau, J. M. Le Goff, A. Cuceu, C. Bolland and J. E. Bautista, *et al.* *Astrophys. J.* **901** (2020) no.2, 153 [[arXiv:2007.08995](#) [astro-ph.CO]].
- [80] N. Khadka and B. Ratra, *Mon. Not. Roy. Astron. Soc.* **502** (2021) no.4, 6140-6156 [[arXiv:2012.09291](#) [astro-ph.CO]].
- [81] N. Khadka and B. Ratra, [[arXiv:2107.07600](#) [astro-ph.CO]].
- [82] E. Ó Colgáin and M. M. Sheikh-Jabbari, *Class. Quant. Grav.* **38** (2021) no.17, 177001 [[arXiv:2102.09816](#) [gr-qc]].
- [83] N. Khadka, O. Luongo, M. Muccino and B. Ratra, [[arXiv:2105.12692](#) [astro-ph.CO]].
- [84] D. Camarena and V. Marra, *Mon. Not. Roy. Astron. Soc.* **504** (2021), 5164-5171 [[arXiv:2101.08641](#) [astro-ph.CO]].
- [85] G. Efstathiou, *Mon. Not. Roy. Astron. Soc.* **505** (2021) no.3, 3866-3872 [[arXiv:2103.08723](#) [astro-ph.CO]].
- [86] F. Melia, *Mon. Not. Roy. Astron. Soc.* **489** (2019) no.1, 517-523 [[arXiv:1907.13127](#) [astro-ph.CO]].
- [87] M. Demianski, E. Piedipalumbo, D. Sawant and L. Amati, *Mon. Not. Roy. Astron. Soc.* **506** (2021) no.1, 903-918 [[arXiv:1911.08228](#) [astro-ph.CO]].
- [88] H. Khoramnezhad, M. Viel, C. Baccigalupi and M. Archidiacono, *JCAP* **07** (2020), 039 [[arXiv:2001.10252](#) [astro-ph.CO]].
- [89] M. Lindner, K. Max, M. Platscher and J. Rezaeck, *JCAP* **10** (2020), 040 [[arXiv:2002.01487](#) [astro-ph.CO]].
- [90] X. Zheng, K. Liao, M. Biesiada, S. Cao, T. H. Liu and Z. H. Zhu, [[arXiv:2002.09909](#) [astro-ph.CO]].
- [91] A. Mehrabi and S. Basilakos, *Eur. Phys. J. C* **80** (2020) no.7, 632 [[arXiv:2002.12577](#) [astro-ph.CO]].
- [92] T. Liu, S. Cao, J. Zhang, M. Biesiada, Y. Liu and Y. Lian, [[arXiv:2005.13990](#) [astro-ph.CO]].
- [93] M. Demianski, E. Lusso, M. Paolillo, E. Piedipalumbo and G. Risaliti, *Front. Astron. Space Sci.* **7** (2020), 69 [[arXiv:2010.05289](#) [astro-ph.CO]].
- [94] J. P. Hu, Y. Y. Wang and F. Y. Wang, *Astron. Astrophys.* **643** (2020), A93 [[arXiv:2008.12439](#) [astro-ph.CO]].
- [95] O. Luongo and M. Muccino, *Astron. Astrophys.* **641** (2020), A174 [[arXiv:2010.05218](#) [astro-ph.CO]].
- [96] S. Cao, J. Ryan, N. Khadka and B. Ratra, *Mon. Not. Roy. Astron. Soc.* **501** (2021) no.1, 1520-1538 [[arXiv:2009.12953](#) [astro-ph.CO]].
- [97] L. Speri, N. Tamanini, R. R. Caldwell, J. R. Gair and B. Wang, *Phys. Rev. D* **103** (2021) no.8, 083526 [[arXiv:2010.09049](#) [astro-ph.CO]].
- [98] O. Luongo and M. Muccino, *Mon. Not. Roy. Astron. Soc.* **503** (2021) no.3, 4581-4600 [[arXiv:2011.13590](#) [astro-ph.CO]].
- [99] M. Muccino, L. Izzo, O. Luongo, K. Boshkayev, L. Amati, M. Della Valle, G. B. Pisani and E. Zaninoni, *Astrophys. J.* **908** (2021) no.2, 181 [[arXiv:2012.03392](#) [astro-ph.CO]].
- [100] X. Li, R. E. Keeley, A. Shafieloo, X. Zheng, S. Cao, M. Biesiada and Z. H. Zhu, [[arXiv:2103.16032](#) [astro-ph.CO]].
- [101] Y. Lian, S. Cao, M. Biesiada, Y. Chen, Y. Zhang and W. Guo, *Mon. Not. Roy. Astron. Soc.* **505** (2021) no.2, 2111-2123 [[arXiv:2105.04992](#) [astro-ph.CO]].
- [102] F. Y. Wang, J. P. Hu, G. Q. Zhang and Z. G. Dai, [[arXiv:2106.14155](#) [astro-ph.HE]].
- [103] A. R. King and G. F. R. Ellis, *Commun. Math. Phys.* **31** (1973), 209-242
- [104] G. F. R. Ellis and H. van Elst, *NATO Sci. Ser. C* **541** (1999), 1-116 [[arXiv:gr-qc/9812046](#) [gr-qc]].
- [105] A. Lewis, [[arXiv:1910.13970](#) [astro-ph.IM]].